Finding Antipodal Point Grasps on Irregularly Shaped Objects

I-Ming Chen and Joel W. Burdick

Abstract—**Two-finger antipodal point grasping of arbitrarily shaped smooth 2-D and 3-D objects is considered. An object function is introduced that maps a finger contact space to the object surface. Conditions are developed to identify the feasible grasping region, $\mathcal{F}$, in the finger contact space. A "grasping energy function," E, is introduced that which is proportional to the distance between two grasping points. The antipodal points correspond to critical points of E in $\mathcal{F}$. Optimization and/or continuation techniques are used to find these critical points. In particular, global optimization techniques are applied to find the "maximal" or "minimal" grasp. Further, modeling techniques are introduced for representing 2-D and 3-D objects using B-spline curves and spherical product surfaces.**

I. Introduction

Two-finger *antipodal point grasps* on 2-D and 3-D smooth objects are considered in this paper. Antipodal points are a pair of points on an object whose normal vectors are collinear and in opposite direction. With appropriate finger contact conditions (point contact with friction for 2-D objects or soft finger contact for 3-D objects [13]) antipodal point grasps guarantee force-closure (FC) [14], [17].

The analysis and planning of multifingered grasps has received considerable attention in the literature. FC grasps on polygonal objects has been studied by many authors [12], [18], [19]. Nguyen [17] developed a geometric test for two-finger FC grasps on both polygonal and polyhedral objects. However, we are interested in curved objects here. Both Chen and Burdick [5] and Faverjon and Ponce [7] extend Nguyen's idea to FC grasps on curved shape objects.

Hong *et al.* [8] first introduced the concept of antipodal point grasps on a smooth object. Their work was motivated by a heuristic approach to planning "finger gaits" in which fingers are placed on or in the neighborhood of antipodal points during the finger repositioning phases of a finger gait. Using a "distance function" on the distance between two contact points, they showed the existence of at least a pair of antipodal points on any smooth shaped objects. Further, for *convex* objects they remarked [8, Prop. 5.5] that the antipodal points could be found by searching for the critical points of their distance function.

In this paper, we introduce an extension of their result to *nonconvex* smooth objects. We also consider in this paper some practical issues in implementing antipodal point finding algorithms, including optimization techniques and object modeling methods. We define a *grasping energy function,* that is proportional to the square of distance between the two finger contacts. This function is identical, modulo a constant, to the distance function of [8]. We show that critical points of this energy function which lie in the *force-closure region* in the *contact configuration* space [5], [7] correspond to pairs of antipodal points on the object surface. For the case of convex bodies considered in [8], the critical points always lie in the force closure regions. However, for the case of nonconvex bodies studied here, the critical points of this function need not be antipodal points. Thus, the search for antipodal points can be reduced to a constrained optimization procedure.

The energy minima and maxima correspond to the *minimal* and *maximal grasps.* Optimization or continuation techniques can be used to find the critical points of the grasping energy function. Here, we use a global optimization scheme, whose acronym is TRUST [4], to find the minimal and maximal grasps. To illustrate a practical implementation of this method, we use B-spline curves and spherical product surfaces to respectively represent the 2-D and 3-D objects.

Section II considers 2-D antipodal point grasping. Section III reviews methods for finding antipodal points. Section IV formulates the 3-D object grasping problem in a manner analogous to Section II. Section V discusses a 2-D and 3-D object representation scheme. Numerical examples are given for both cases.

Manuscript received January 22, 1992; revised December 22, 1992.

The authors are with the Division of Engineering and Applied Science, California Institute of Technology, Mail Stop 104-44, Pasadena, CA 91125.

IEEE Log Number 9210238.

II. Two-Dimensional Object Antipodal Point Grasps

A. Preliminaries

We assume that the boundary of a grasped planar object is a smooth and closed curve. Attach a coordinate frame, O, to the object. The object boundary can be described by a 1-to-1 parametric function:

$$\boldsymbol{p}(u) = [x(u), y(u)]^T, \qquad u \in \mathbf{S}^1 \tag{1}$$

where u is called a *contact variable* and S^1 is a 1-sphere (unit circle); $\boldsymbol{p}(u_0) = [x(u_0), y(u_0)]^T$ represents a contact location, in frame O, on the object at u_0. Since the object function is 1-to-1, u_0 can represent a contact, instead of $\boldsymbol{p}(u_0)$. We assume $\boldsymbol{p}(u)$ is at least once differentiable. Therefore, a unit tangent vector $\boldsymbol{t}(u_0)$, and a unit outward pointing normal vector $\boldsymbol{n}(u_0)$, exist at u_0.

$$\boldsymbol{t}(u_0) = \frac{\boldsymbol{p}'(u_0)}{\|\boldsymbol{p}'(u_0)\|} \tag{2}$$

where $\boldsymbol{p}'(u_0) = (d\boldsymbol{p})/(du)|_{u_0}$.

Definition 1—Antipodal Points [11]*:* Two contacts, u_1 and u_2, which satisfy the following conditions are called *antipodal points:*

$$[\boldsymbol{p}(u_1) - \boldsymbol{p}(u_2)] \cdot \boldsymbol{t}(u_1) = 0 \tag{3}$$

$$[\boldsymbol{p}(u_2) - \boldsymbol{p}(u_1)] \cdot \boldsymbol{t}(u_2) = 0 \tag{4}$$

$$\boldsymbol{n}(u_1) + \boldsymbol{n}(u_2) = 0. \tag{5}$$

Definition 2—Contact Configuration [8]*:* The ordered pair $\boldsymbol{q} = (u_1, u_2)$, which represents the location of two point contacts on the object, with $u_1 \neq u_2$, for $u_1, u_2 \in \mathbf{S}^1$, is called a *contact configuration* of a 2-contact grasp.

Definition 3—Contact Configuration Space for 2-D Objects: Let $T^2 = S^1 \times S^1$ and $\Delta = \{(u_1, u_2) | u_1 = u_2 \in \mathbf{S}^1\}$. The set

$$\mathcal{C}_2 = T^2 \backslash \Delta \tag{6}$$

is called the 2-contact configuration space (or 2-contact C-space). Δ represents all physically unrealizable contact configurations in which two fingers occupy the same location on the object. Thus, $\mathcal{C}_2$ represents all possible 2-finger grasps on the object.

B. Force-Closure Regions and Curves

We also assume that: 1) the finger contact is point contact with friction (PCWF); and 2) the contact friction is Coulomb friction, with friction coefficient μ which is everywhere constant on the object. The friction at $\boldsymbol{p}(u_0)$ defines a conical region, denoted by $\mathcal{S}(u_0)$, called the friction cone. Sliding between the finger and the object will not occur if the force exerted by the finger lies in the friction cone. For planar objects, $\mathcal{S}(u_0)$ consists of two sectors: one extending outside of the object termed the *positive friction cone* $\mathcal{S}^+(u_0)$ and the other extending inward termed the *negative friction cone* $\mathcal{S}^-(u_0)$ (see Fig. 1). A contact force exerted by the finger contact at u_0 is called *feasible* if it lies in the negative friction cone $\mathcal{S}^-(u_0)$. A two-finger grasp is said to be force-closure if any external force and moment

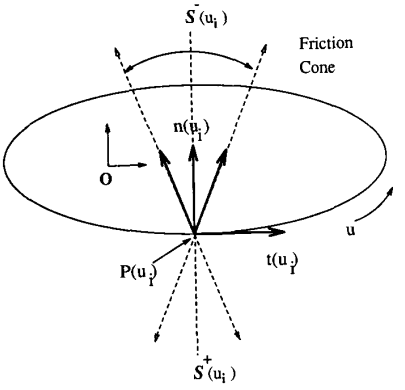

Fig. 1. Positive and negative friction cone.

on the object can be balanced by a positive linear combination of two feasible contact forces exerted by the fingers [13]. Nguyen [17] showed that a 2-finger force-closure grasp (or FC grasp) $\boldsymbol{q} = (u_1, u_2)$ can be achieved if and only if the line connecting $\boldsymbol{p}(u_1)$ and $\boldsymbol{p}(u_2)$ lies inside both $\mathcal{S}(u_1)$ and $\mathcal{S}(u_2)$. There are two possible geometric conditions satisfying this statement:

Definition 4—Squeezing and Expanding Force-Closure Grasps: Denote the line connecting contact points u_1 and u_2 by $\overline{u_1u_2}$. If $\overline{u_1u_2}$ falls inside both $\mathcal{S}^-(u_1)$ and $\mathcal{S}^-(u_2)$, the FC grasp $\boldsymbol{q}$ is called a *squeezing grasp* (see Fig. 2). If $\overline{u_1u_2}$ falls inside both $\mathcal{S}^+(u_1)$ and $\mathcal{S}^+(u_2)$, the FC grasp $\boldsymbol{q}$ is called an *expanding grasp* (see Fig. 3). Convex objects can be grasped by squeezing grasps only. Non-convex objects can be grasped by squeezing and possibly expanding grasps as well. A squeezing FC grasp, $\boldsymbol{q}$, satisfies:

$$\boldsymbol{n}(u_1) \cdot \frac{\boldsymbol{p}(u_1) - \boldsymbol{p}(u_2)}{\|\boldsymbol{p}(u_1) - \boldsymbol{p}(u_2)\|} > c_f \tag{7}$$

$$\boldsymbol{n}(u_2) \cdot \frac{\boldsymbol{p}(u_2) - \boldsymbol{p}(u_1)}{\|\boldsymbol{p}(u_2) - \boldsymbol{p}(u_1)\|} > c_f. \tag{8}$$

while an expanding grasp, $\boldsymbol{q}$, satisfies:

$$\boldsymbol{n}(u_1) \cdot \frac{\boldsymbol{p}(u_1) - \boldsymbol{p}(u_2)}{\|\boldsymbol{p}(u_1) - \boldsymbol{p}(u_2)\|} < -c_f \tag{9}$$

$$\boldsymbol{n}(u_2) \cdot \frac{\boldsymbol{p}(u_2) - \boldsymbol{p}(u_1)}{\|\boldsymbol{p}(u_2) - \boldsymbol{p}(u_1)\|} < -c_f \tag{10}$$

where $c_f = \cos(\tan^{-1}\mu)$. The inequalities (7)–(10) define regions in $\mathcal{C}_2$ called *force-closure regions,* or feasible grasping regions [5], in which the grasps are force-closure. Let $\mathcal{F}^-$ denote all grasps in $\mathcal{C}_2$ satisfying (7) and (8) and $\mathcal{F}^+$ the grasps satisfying (9) and (10). $\mathcal{F} = \mathcal{F}^- \cup \mathcal{F}^+$ (where $\mathcal{F}^- \cap \mathcal{F}^+ = \emptyset$) is the set of all force-closure grasps. The force-closure curves (FC curves) that bound the FC regions in $\mathcal{C}_2$ are the zero sets of the functions obtained by replacing the inequalities (7) to (10) by equalities. Note that this method of finding FC-regions extends to 3-D, whereas the method of [7], which relies upon the cross product of the friction cone normal and edge vectors, cannot. A 3-D object friction cone cannot be described by a linear combination of finite vectors, hence, the cross product method is no longer valid.

C. A Grasping Energy Function

A "grasping energy function" $E : \mathcal{C}_2 \rightarrow R$ is defined as

$$E(u_1, u_2) = \frac{1}{2}\kappa\|\boldsymbol{p}(u_1) - \boldsymbol{p}(u_2)\|^2 \tag{11}$$

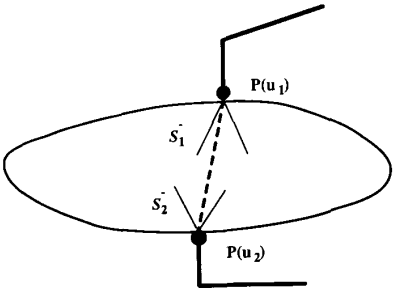

Fig. 2. A squeezing grasp.

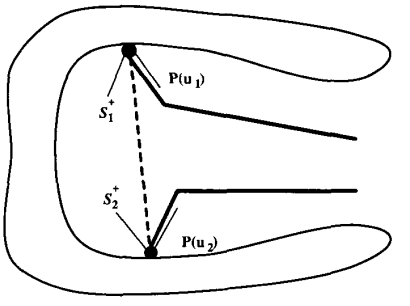

Fig. 3. An expanding grasp.

where E can be interpreted as the energy of a spring, with spring constant κ, connecting u_1 and u_2. E is continuous and once differentiable.

Proposition 1: A pair of antipodal points, u_1 and u_2, correspond to a critical point of E. Conversely, only critical points of E lying in $\mathcal{F}$ correspond to a pair of antipodal points.

Proof: Let u_1 and u_2 be antipodal points. Substituting (2) into (3) and (4), we get

$$[\boldsymbol{p}(u_1) - \boldsymbol{p}(u_2)] \cdot \frac{\boldsymbol{p}'(u_1)}{\|\boldsymbol{p}'(u_1)\|} = 0 \tag{12}$$

$$[\boldsymbol{p}(u_2) - \boldsymbol{p}(u_1)] \cdot \frac{\boldsymbol{p}'(u_2)}{\|\boldsymbol{p}'(u_2)\|} = 0. \tag{13}$$

Since $\|\boldsymbol{p}'(u)\| \neq 0$, by smoothness of the boundary curve:

$$\kappa[\boldsymbol{p}(u_1) - \boldsymbol{p}(u_2)] \cdot \boldsymbol{p}'(u_1) = \frac{\partial E}{\partial u_1} = 0 \tag{14}$$

$$\kappa[\boldsymbol{p}(u_2) - \boldsymbol{p}(u_1)] \cdot \boldsymbol{p}'(u_2) = \frac{\partial E}{\partial u_2} = 0. \tag{15}$$

Thus, $\boldsymbol{q} = (u_1, u_2)$, is a critical point of E. Conversely, for nonconvex objects, *a critical point of E does not necessarily satisfy* (5), and is therefore not necessarily an antipodal point. Any grasp, $\boldsymbol{q}$, lying in $\mathcal{F}$ satisfies either (7) and (8) or (9) and (10). Note that for any $(u_1, u_2) \in \mathcal{F}$, the angle between two normal vectors $\boldsymbol{n}(u_1)$ and $\boldsymbol{n}(u_2)$ is between $\pi - 2\tan^{-1}\mu$ and π. If $\boldsymbol{q}^* = (u_1^*, u_2^*)$ is a critical point of E and $q^* \in \mathcal{F}$, then $\boldsymbol{n}(u_1^*), \boldsymbol{n}(u_2^*)$ will be collinear and in opposite directions. Hence, (3)–(5) are all satisfied. $\boldsymbol{q}^*$ represents an antipodal point grasp on the object. ■

Since E is differentiable over $\mathcal{C}_2$ (which is compact), E must achieve both a maximum, at $\boldsymbol{q}_{\max}$, and a minimum, at $\boldsymbol{q}_{\min}$, in $\mathcal{C}_2$. $\boldsymbol{q}_{\max}$ and $\boldsymbol{q}_{\min}$ are respectively termed the "maximal" and "minimal" grasps. Nonconvex objects can have critical points which are local minima and maxima of E. The properties of these critical points depend upon the local object geometry near the antipodal points. Let $\boldsymbol{q}^* = (u_1^*, u_2^*)$ denote an antipodal point pair. If the object is

convex (concave) at u_1^* and u_2^*, $E(u_1^*, u_2^*)$ will be a local maximum (minimum). If the object is convex at one antipodal point and concave at the other, the critical point may be a saddle point, local minimum, or local maxima, depending on the relative object curvature at u_1^* and u_2^*. E is necessarily convex (resp. concave) at the maximal (minimal) antipodal points.

These local properties can be used to differentiate between different antipodal grasp choices. The previous and ensuing discussion neglects the 3-D volumetric properties of the fingertips. An automated grasp planner should check for interference between the finger and the object. If the grasping fingertips are convex, the maximal grasp does not require additional calculations which check for geometric interference. In principle, simple parallel jaw grippers could be used to grasp at the maximal grasp without complex calculations. However, it is known that the maximal two-fingered grasp may be less "stable" [15] than other antipodal point grasps. Conversely, the minimal grasp is a more stable or immobile grasp. It may be more desirable, even if additional computations are required to check for interference between the object and fingers. The choice between locally maximal or minimal antipodal point grasps is thus a function of other task requirements.

III. Planning Antipodal Point Grasps—Critical Points Finding Algorithms

Proposition 1 suggests that antipodal points can be found by searching for the critical points of E in the FC regions. For many practical applications, we are more interested in finding the subset of critical points which are either minima or maxima of E. In these case, we can the formulate antipodal point search problem as a constrained optimization problem:

$$\begin{aligned} \max \quad & E^*(u_1, u_2) = \frac{1}{2}\kappa \|\boldsymbol{p}(u_1) - \boldsymbol{p}(u_2)\|^2 \\ \text{subject to} \quad & (u_1, u_2) \in \mathcal{F} \subset \mathcal{C}_2 \end{aligned} \tag{16}$$

where $E(u_1, u_2) = E^*(u_1, u_2)$ if one is interested in locally maximal grasps, or $E(u_1, u_2) = -E^*(u_1, u_2)$ if locally minimal grasps are of interest. Any suitable constrained optimization method, such as the method of Lagrange multipliers, constrained Newton or quasi-Newton methods, or successive quadratic programming [2], can be used to solve (16). In most cases, the constraints arise only from force closure. However, in some practical cases, portions of the object surface maybe occluded by nearby objects, or not visible to a robot vision system which generates object models. In such cases, additional constraints can be added to exclude these regions in the optimization process.

The aforementioned optimization methods have only local convergence properties. Thus, the antipodal points found by these methods will depend on the procedure's initial conditions. Multiple random start methods [3] can be used to find all of the local critical points. Alternatively, constrained global optimization techniques, such as simulated annealing [10] or interval analysis methods [16] can be used to find the globally minimal or maximal grasp. In this work, the global maximum of E is found using a recently developed global optimization algorithm, termed TRUST (see [4] for details). This method is simple to implement and has been found to be substantially faster than other global optimization methods in benchmark tests. TRUST uses a novel "tunneling" method which finds the global extrema by repeatedly escaping local extrema. Thus, on the way to finding the global solution, many local critical points, which correspond to feasible antipodal grasping points, are identified. However, all critical points are not found on the way to the global optimum.

These methods suggested above are most useful if the antipodal points are isolated in $\mathcal{C}_2$. However, when the object contains parallel edges or faces, for example, the antipodal points will not be isolated point sets. In these cases, the critical points of E can be found using continuation techniques developed for numerical bifurcation analysis [9].

From a set of antipodal points, which are found using a multiple random start or as intermediate steps of a tunneling global optimization, one can select an antipodal point pair based on additional considerations. For example, interference between fingertips, or a distance between antipodal points (which might exceed the greatest dimension of the hand workspace) can be used to cull antipodal points from the feasible set.

IV. 3-D Object Grasping

This section extends the methodology for 2-D object grasping to 3-D object grasping. We assume the object is devoid of holes and homeomorphic to a sphere. The surface of the object can be described by a 1-to-1 function:

$$\boldsymbol{s}(\boldsymbol{u}) = [x(\boldsymbol{u}), y(\boldsymbol{u}), z(\boldsymbol{u})]^T, \qquad \boldsymbol{u} \in \mathbf{S}^2 \tag{17}$$

where $\boldsymbol{u} \in \mathbf{S}^2$ is a contact variable. Since the function is also 1-to-1, we can use $\boldsymbol{u}_0$ instead of $\boldsymbol{s}(\boldsymbol{u}_0)$ to represent a contact point on the object. A contact configuration of a 2-finger grasp is defined to be $\boldsymbol{q} = (\boldsymbol{u}_1, \boldsymbol{u}_2)$ with $\boldsymbol{u}_1 \neq \boldsymbol{u}_2$ and $\boldsymbol{u}_1, \boldsymbol{u}_2 \in \mathbf{S}^2$. If $\Gamma = \{(\boldsymbol{u}_1, \boldsymbol{u}_2) | \boldsymbol{u}_1 = \boldsymbol{u}_2 \in \mathbf{S}^2\}$ denotes the set of physically unrealizable contact configurations, the contact configuration space, $\mathcal{D}_2$, of 2-finger grasp on a 3-D object is

$$\mathcal{D}_2 = S^2 \times S^2 \backslash \Gamma. \tag{18}$$

For 3-D object grasping, we assume: 1) a soft-finger contact model (i.e., the finger can exert torque about the contact normal); 2) that friction is Coulomb friction, with coefficient μ, which is everywhere constant; and 3) a constant rotational friction coefficient γ. As before, we call the friction cone extending outside of the object $\mathcal{S}^+(\boldsymbol{u}_0)$ and the one inside the object $\mathcal{S}^-(\boldsymbol{u}_0)$. Nguyen [17] also showed that for 3-D object, a two-finger grasp, $\boldsymbol{q} = (\boldsymbol{u}_1, \boldsymbol{u}_2)$, with soft-finger contact model will be force-closure if and only if the line connecting the $\boldsymbol{p}(\boldsymbol{u}_1)$ and $\boldsymbol{p}(\boldsymbol{u}_2)$ lies strictly inside both friction cones $\mathcal{S}^-(\boldsymbol{u}_1)$ and $\mathcal{S}^-(\boldsymbol{u}_2)$ (or $\mathcal{S}^+(\boldsymbol{u}_1)$ and $\mathcal{S}^+(\boldsymbol{u}_2)$).

The definition of antipodal points on a 3-D object is similar to (3) to (5), except the tangent vectors $\boldsymbol{t}(\boldsymbol{u}_1)$, and $\boldsymbol{t}(\boldsymbol{u}_2)$ can be any vectors in the tangent spaces at $\boldsymbol{u}_1$ and $\boldsymbol{u}_2$. The squeezing and expanding force closure grasps are also similar to the 2-D case. One can derive inequalities analogous to (7)–(10) which define FC grasping regions: $g_1^-(\boldsymbol{u}_1, \boldsymbol{u}_2) > 0, g_2^-(\boldsymbol{u}_1, \boldsymbol{u}_2) > 0, g_1^+(\boldsymbol{u}_1, \boldsymbol{u}_2) < 0$, and $g_2^+(\boldsymbol{u}_1, \boldsymbol{u}_2) < 0$. Let

$$\begin{aligned} \mathcal{G}^- &= \{(\boldsymbol{u}_1, \boldsymbol{u}_2) | g_1^- > 0, g_2^- > 0; (\boldsymbol{u}_1, \boldsymbol{u}_2) \in \mathcal{D}_2\} \\ \mathcal{G}^+ &= \{(\boldsymbol{u}_1, \boldsymbol{u}_2) | g_1^+ < 0, g_2^+ < 0; (\boldsymbol{u}_1, \boldsymbol{u}_2) \in \mathcal{D}_2\} \end{aligned}$$

where $\mathcal{G}^-$ and $\mathcal{G}^+$ represent all squeezing and expanding force closure grasps in $\mathcal{D}_2$. The two-fingered FC grasping region is the set $\mathcal{G} = \mathcal{G}^- \cup \mathcal{G}^+ \subset \mathcal{D}_2$.

A 3-D grasping energy function, $E_3 : \mathcal{D}_2 \rightarrow R$ can be defined as:

$$E_3(\boldsymbol{u}_1, \boldsymbol{u}_2) = \frac{1}{2}\kappa \|\boldsymbol{s}(\boldsymbol{u}_1) - \boldsymbol{s}(\boldsymbol{u}_2)\|^2 \tag{19}$$

Proposition 2: A pair of antipodal points, $\mathbf{u}_1$ and $\mathbf{u}_2$, on a 3-D object correspond to a critical point of E_3. Conversely, critical points of E_3 in the FC-region $\mathcal{G}$, correspond to antipodal point pairs.

The proof of this proposition is completely analogous to that of Proposition 1. However, the optimization of E_3 is difficult to implement because the $\mathcal{D}_2$ does not admit a global parametrization.

V. Representations of Objects

A. 2-D Objects

It is not always practically easy to find a smooth mapping $\boldsymbol{p}: \mathbf{S}^1 \rightarrow \mathbf{R}^2$ to model the shape of a curved object. For illustration purposes, we here use cubic B-spline curves that are frequently used in computer graphics applications to represent the boundaries of 2-D objects. This method is computationally efficient, produces surface with satisfactory smoothness, and can be used to approximate nearly any smooth object with arbitrary precision. For more detailed treatment of B-spline curves, please refer to [22].

A cubic B-spline curve is a collection of piecewise continuous parametric cubic polynomial curve segments whose derivatives are continuous at "knot points." If the parametric intervals in all segments are equal, the curve is called a *uniform cubic B-spline curve.* Every segment i in the uniform cubic B-spline curve has the following form:

$$\boldsymbol{p}_i(t_i) = \boldsymbol{a}_i t_i^3 + \boldsymbol{b}_i t_i^2 + \boldsymbol{c}_i t_i + \boldsymbol{d}_i \tag{20}$$

where $\boldsymbol{a}_i, \boldsymbol{b}_i, \boldsymbol{c}_i, \boldsymbol{d}_i \in \mathbf{R}^2$ are coefficients of the polynomial $\boldsymbol{p}_i$ and $t_i \in I = [0,1]$ is the local curve parameter. Non-uniform cubic B-spline curves can also be applied to model the object boundary. However, for simplicity, we use uniform cubic B-spline curves in this paper. Non-uniform splines can be converted to uniform splines through a resampling process. A process for computing the b-spline parameters from experimental data can be found in [22].

Suppose that an object is described by a uniform B-spline curve of n segments. If the local parameter intervals are normalized to [0,1], then a single global parameter u, defined on the interval $I_n \equiv [0, n]$, can be defined to accumulate the values of local curve parameters $\{t_i\}$. The object boundary is usually a closed curve, hence, the two end points of the B-spline curve coincide.

Example 1: Fig. 4 shows an object modeled by a cubic B-spline curve of eight segments. The global parameter interval is $I_8 = [0, 8]$. Fig. 5 shows the FC-regions in $\mathcal{C}_2$. Since the boundary curve is a cubic polynomial, E is a polynomial of degree 6, as shown in Fig. 6 (where $\kappa = 1$). Table I lists the global maximum and local extrema of E found by TRUST. Since E is symmetric with respect to the line $u_1 = u_2$, only extrema with $u_1 > u_2$ are listed. The corresponding maximal and antipodal point grasp locations are shown in Fig. 4. When part of the object is occluded by nearby obstacles or unviewable by vision sensors, the object boundary can be modeled by one or more open cubic B-spline curves. We can still use the accumulated-value global parameter method for each B-spine curve and consider all possible combinations of fingertip locations on any of the open curves. The constrained optimization formulation for finding antipodal points still holds.

B. 3-D Objects

Local models for 3-D object surfaces can be developed using many techniques, such as B-spline surfaces, Bezier surfaces, etc. [6], [22]. The entire object surface is described by a collection of surface patches. Here we use *spherical product surfaces* to globally represent artificial and natural objects. The spherical product was first introduced by Barr [1] to represent a family of parametrized

TABLE I
Extrema and Corresponding Antipodal Points

Extrema	Contact Config.	Antipodal Points	
Global Max(△)	(3.999, 0.071)	(−0.100, −0.900)	(0.020, 0.801)
Local Max (◇)	(6.070, 2.003)	(−0.704, 0.023)	(0.700, 0.098)
Local Min(⋆)	(5.245, 1.027)	(−0.407, −0.272)	(0.312, 0.488)
Local Min (□)	(7.005, 2.875)	(−0.398, 0.403)	(0.370, −0.322)

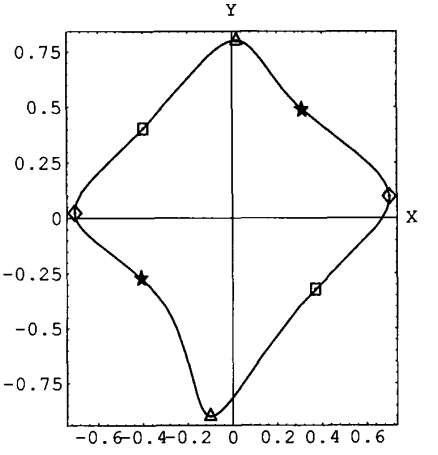

Fig. 4. A 2-D object for Example 1.

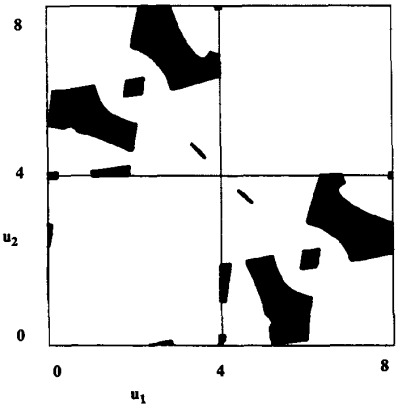

Fig. 5. Force-closure region with $\mu = 0.3$.

trigonometric 3-D surfaces called *superquadric surfaces.* The basic form of a 3-D spherical product surface is defined as [1]:

$$\boldsymbol{s}(u,v) = \boldsymbol{f}(u) \otimes \boldsymbol{g}(v) - [f_1(u)g_2(v), f_1(u)g_2(v), f_2(u)] \tag{21}$$

where $\boldsymbol{f}(u)$ and $\boldsymbol{g}(u)$ are 2-D curves:

$$\boldsymbol{f}(u) = [f_1(u), f_2(u)], \qquad u \in I_u \equiv [u_0, u_1] \tag{22}$$

$$\boldsymbol{g}(v) = [g_1(v), g_2(v)], \qquad v \in I_v \equiv [v_0, v_1] \tag{23}$$

where $\boldsymbol{f}(u)$ and $\boldsymbol{g}(v)$ are parametric trigonometric curves in [1]. To

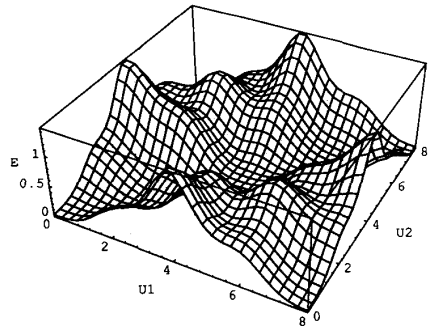

Fig. 6. The grasping energy function E.

represent a richer set of objects, we extend this definition to use B-spline curves instead: let $\boldsymbol{f} : I_u \equiv I_m \rightarrow R^2$ be an *open* cubic B-spline curve of m segments and $\boldsymbol{g} : I_v \equiv I_n \rightarrow \mathbf{R}^2$ a *closed* cubic B-spline curve of n segments. To guarantee object surface smoothness, $\boldsymbol{f}(u)$ and $\boldsymbol{g}(v)$ must satisfy the following conditions:

(R-1) $\boldsymbol{f}(u)$ and $\boldsymbol{g}(v)$ must be regular curves.

(R-2) The curve $\boldsymbol{f}(u)$ intersects the y-axis at $\boldsymbol{f}(0)$ and $\boldsymbol{f}(m)$ only. The tangents $\boldsymbol{f}'(0)$ and $\boldsymbol{f}'(m)$ must have zero slope.

(R-3) The tangent vector and the position vector of a point on $\boldsymbol{g}(v)$ are not parallel, i.e., $\boldsymbol{g}(v) \neq \alpha \boldsymbol{g}'(v)$ for some $\alpha \neq 0$, or $g_1 g_2' - g_1' g_2 \neq 0$.

With these restrictions, the generalized spherical product surfaces can be used as primitive computer models of real object surfaces [20]. By comparing with range data of real objects, primitive models can be deformed approximately into the shape of real objects via a series of linear and nonlinear transformations such as linear stretching, tapering, or quadratic bending [21]. This is a very versatile object modeling system for real time implementation of object grasping. For simplicity, we investigate grasping on the primitive object form, i.e., spherical product surfaces without distortion, in this paper.

The spherical produce, which maps $I_m \times I_n$ onto a surface diffeomorphic to $\mathbf{S}^2$, is not a 1-to-1 mapping because the two polar points, $\boldsymbol{p_n} = \boldsymbol{s}(0, v)$ and $\boldsymbol{p_s} = \boldsymbol{s}(m, v), v \in I_n$, are actually degenerate curves. However, it can be shown [6] that the normal vectors at the polar points are well defined and continuous in the neighborhoods of $\boldsymbol{p_n}$ and $\boldsymbol{p_s}$.

The domain of the spherical product surface is $I_u \times I_v$, so the contact C-space becomes $\mathcal{D}_2^* = I_u \times I_v \times I_u \times I_v$, which is topologically different from $\mathcal{D}_2$. A grasp configuration is thus denoted by $\boldsymbol{q} = (u_1, v_1, u_2, v_2)$. Let $\boldsymbol{s}_u \equiv (\partial \boldsymbol{s})/(\partial u)|_{(u_0, v_0)}$ and $\boldsymbol{s}_v \equiv (\partial \boldsymbol{s})/(\partial v)|_{(u_0, v_0)}$ denote surface tangent vectors at $\boldsymbol{p}_0 = \boldsymbol{s}(u_0, v_0)$ along u and v direction respectively. The unit outward normal vector at $\boldsymbol{p}_0$ is

$$\boldsymbol{n}(u_0, v_0) = \pm \frac{\boldsymbol{s}_u \times \boldsymbol{s}_v}{\|\boldsymbol{s}_u \times \boldsymbol{s}_v\|} \tag{24}$$

except at $\boldsymbol{p_n}$ and $\boldsymbol{p_s}$. The sign of $\boldsymbol{n}$ depends on the directions of parametrization of curves $\boldsymbol{f}(u)$ and $\boldsymbol{g}(v)$. The unit outward normal vectors at polar points are $\boldsymbol{n}_{P_n} = [0, 0, 1]$ and $\boldsymbol{n}_{P_s} = [0, 0, -1]$.

We divide the finger contact space $\mathcal{D}_2^* = \{(u_1, v_1, u_2, v_2) | 0 \leq u_i \leq m, 0 \leq v_i \leq n, i = 1, 2\}$ into six subsets to determine the FC regions in $\mathcal{D}_2^*$:

$$\mathcal{D}_{21}^* = \{\boldsymbol{u} | 0 < u_i < m, 0 \leq v_i \leq n, i = 1, 2\}$$
$$\mathcal{D}_{22}^* = \{\boldsymbol{u} | u_1 = 0, 0 < u_2 < m, 0 \leq v_i \leq n, i = 1, 2\}$$
$$\mathcal{D}_{23}^* = \{\boldsymbol{u} | u_1 = m, 0 < u_2 < m, 0 \leq v_i \leq n, i = 1, 2\}$$
$$\mathcal{D}_{24}^* = \{\boldsymbol{u} | u_2 = 0, 0 < u_1 < m, 0 \leq v_i \leq n, i = 1, 2\}$$
$$\mathcal{D}_{25}^* = \{\boldsymbol{u} | u_2 = m, 0 < u_1 < m, 0 \leq v_i \leq n, i = 1, 2\}$$
$$\mathcal{D}_{26}^* = \{(0, v_1, 0, v_2), (0, v_1, m, v_2), (m, v_1, 0, v_2), (m, v_1, m, v_2) | 0 \leq v_i \leq n, i = 1, 2\}$$

where $\mathcal{D}_{21}^*$ represents all two-finger grasps which do not include a polar point; $\mathcal{D}_{22}^*$ and $\mathcal{D}_{23}^*$ represent grasp configurations where finger 1 is located at $\boldsymbol{p_n}$ or $\boldsymbol{p_s}$ while finger 2 is located anywhere except at the polar points; $\mathcal{D}_{24}^*$ and $\mathcal{D}_{25}^*$ are similar to $\mathcal{D}_{22}^*$ and $\mathcal{D}_{23}^*$ with finger 1 and finger 2 switching roles. $\mathcal{D}_{26}^*$ represents the four possible contacts of fingers 1 and 2 at $\boldsymbol{p_n}$ and $\boldsymbol{p_s}$. The FC regions, $\mathcal{G}_i^*$, in each subset $\mathcal{D}_{2i}^*$ are derived by substituting (24), $\boldsymbol{n}_{P_n}$, and $\boldsymbol{n}_{P_s}$ into (7) to (10). The entire FC set in $\mathcal{D}_2^*$ is the union of FC regions in every subset, i.e., $\mathcal{G}^* = \cup_{i=1}^{6} \mathcal{G}_i^*$. Antipodal points can be found by finding all critical points of (19) lying in $\mathcal{G}^*$. The constrained critical point finding methods discussed in Section III are applied to each subset $\mathcal{D}_{2i}^*$ separately.

Example 2: Fig. 7 shows a spherical product surface $\boldsymbol{f}(u) \otimes \boldsymbol{g}(v)$. The result of using TRUST in every subset of $\mathcal{D}_2^*$ is listed in Table II and the corresponding antipodal point grasps are shown in Figs. 7 and 8. Because of symmetry, we list grasps with $u_1 < u_2$ only.

TABLE II
EXTREMA AND CORRESPONDING ANTIPODAL POINTS

Contact Configuration	Antipodal Points	
	Global Max (△)	
(1.39, 0.07, 2.95, 4.00)	(0.01, 0.48, 0.21)	(−0.07, −0.64, −0.48)
	Local Max (○)	
(1.44, 4.00, 2.98, 0.07)	(−0.06, −0.55, 0.20)	(0.01, 0.56, −0.49)
	Local Max (□)	
(1.10, 2.01, 3.16, 6.07)	(0.37, −0.05, −0.27)	(−0.44, −0.01, −0.56)
	Local Max (+)	
(1.10, 6.07, 3.16, 2.00)	(−0.38, 0.01, 0.28)	(0.44, 0.06, −0.59)
	Local Max (⋆)	
(0.0, 0.0, 4.0, 2.0)	(0.0, 0.0, 0.4)	(0.0, 0.0, −0.7)

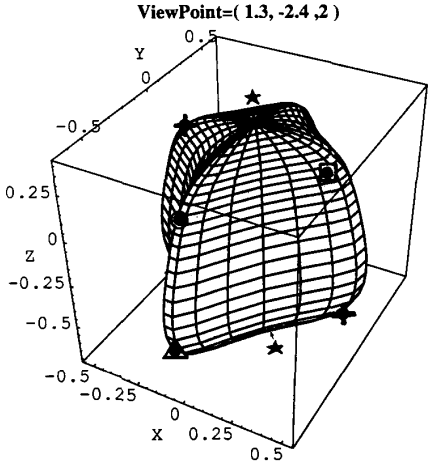

Fig. 7. A 3-D object for Example 2.

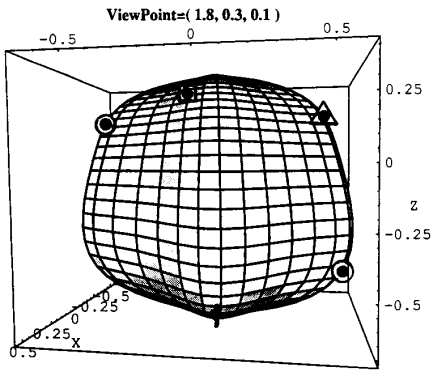

Fig. 8. Different viewpoint.

Note that all these grasps correspond to grasping energy minima or maxima. Antipodal point grasps correspond to saddles of E_3 are not listed here because TRUST will "escape" those saddle points during the optimizing process.

VI. Conclusion

We considered in this paper some practical issues in the implementation of antipodal point grasp finding algorithms on 2-D and 3-D smooth nonconvex objects. A simple grasping energy function was introduced, and it was shown that all antipodal points on the object correspond to the critical points of the energy function in the force-closure regions in contact configuration space. Thus, finding the antipodal points is equivalent to a constrained optimization procedure. For the example, we used a particular global optimization scheme termed TRUST. We also discussed the application of other methods and their relative merits. Our analysis included both squeezing and expanding grasps, which occur for non-convex object. This approach can be used with any object whose boundary can be described by continuous functions. In this paper we introduced a modeling method based on B-spline curves and an extension of spherical product surfaces. These modeling techniques can exactly model or closely approximate a wide variety of artificial and natural object forms. Further, these B-spline modeling methods are well suited to the generation of object models from computer vision data. However, other modeling schemes can be similarly used.

References

[1] A. H. Barr, "Superquadrics and angle-preserving transformations," *IEEE Comput. Graphics and Applications,* vol. 1, pp. 11–23, 1981.
[2] D. P. Bertsekas, in *Constrained Optimization and Lagrange Multiplier Methods.* New York, NY: Academic, 1982.
[3] H. A. Bremermann, "A method of unconstrained global optimization," *Math. Biosci.* vol. 9, pp. 1–15, 1970.
[4] B. Cetin, J. Barhen and J. Burdick, "Terminal repeller sub-energy tunneling (TRUST) for fast global optimization," to appear in *J. Optimization Theory and Applications.*
[5] I. M. Chen and J. Burdick, "Finding antipodal point grasps on irregularly shaped objects," in *Proc. IEEE Int. Conf. Robotics Automat.,* Nice, France, 1992, pp. 2278–2283.
[6] D. Faux and M. J. Pratt, *Computational Geometry for Design and Manufacturing.* Ellis Horwood, 1979.
[7] B. Faverjon and J. Ponce, "On computing two-finger force-closure grasps of curved 2D objects," in *Proc. IEEE Int. Conf. Robotics Automat.,* Sacramento, CA, 1991, pp. 424–429.
[8] J. Hong, G. Lafferriere, B. Mishra and X. Tan, "Fine manipulation with multifinger hands," in *Proc. IEEE Int. Conf. Robotics Automat.,* Cincinatti, OH, 1990, pp. 1568–1573.
[9] H. B. Keller, in *Lectures on Numerical Methods in Bifurcation Problems.* New York, NY: Springer-Verlag, 1987.
[10] S. Kirkpatrick, C. D. Gelatt and M. P. Vecchi, "Optimization by simulated annealing," *Science,* vol. 220, pp. 671–680, 1983.
[11] N. H. Kuiper, "Double Normals of a Convex Body," *Israel J. Math.,* vol. 2, pp. 71–80, 1964.
[12] X. Markenscoff and C. H. Papadimitriou, "Optimum grip of a polygon," *Int. J. Robotic Res.,* vol. 8, no. 2, pp. 17–29, 1989.
[13] M. Mason and J. K. Salisbury, *Robot Hands and the Mechanics of Manipulation.* Cambridge, MA: MIT Press, 1985.
[14] B. Mishra, J. Schwartz and M. Sharir, "On the existence and synthesis of multifinger positive grips," *Algorithmica,* vol. 2, pp. 541–558, 1987.
[15] D. J. Montana, "Contact stability for two-fingered grasps," *IEEE Trans. Robotics Automat.,* vol. 8, no. 4, pp. 421–430, 1992.
[16] R. E. Moore, in *Interval Analysis.*\quad Englewood Cliffs, NJ: Prentice Hall, 1966.
[17] V. Nguyen, "Constructing force-closure grasps," *Int. J. Robotic Res.* vol. 7, no. 3, pp. 3–16, 1988.
[18] T. Omata, "Fingertip positions of a multifingered hand," in *Proc. IEEE Int. Conf. Robotics Automat.,* Cincinatti, OH, 1990, pp. 1562–1567.
[19] Y. C. Park and G. P. Starr, "Grasp synthesis of polygonal objects," in *Proc. IEEE Int. Conf. Robotics Automat.,* Cincinatti, OH, 1990, pp. 1574–1580.
[20] A. Pentland, "Perceptual organization and the representation of natural form," *Artificial Intell.* vol. 28, pp. 293–331, 1986.
[21] A. Pentland and R. Bolles, "Learning and recognition in natural environments," in *Robotics Science,* M. Brady, Ed. Cambridge, MA: MIT Press, 1989, pp. 164–207.
[22] F. Yamaguchi, *Curves and Surfaces in Computer Aided Geometry Design.* New York: Springer-Verlag, 1988.

A Tactile Sensor System for Universal Joint Sections of Manipulators

Yoji Yamada, Kazuhisa Shin, Nuio Tsuchida, and Mataji Komai

Abstract—**It is very difficult to place tactile sensors around revolute joints of manipulators, since those joints and surrounding surfaces are not stationary and thus they remain insensitive to contact with obstacles. This interferes with the introduction of sensors for collision avoidance control in manipulators. This paper deals with a tactile sensor system for universal joint sections of manipulators in order to detect collisions with obstacles. Its unique characteristic is the ability to detect, in one sampling period, the positions of more than one collision despite having only one signal line. It is achieved by making use of the resonance phenomenon of the sensor circuit, and all sensor elements can be distinguished from one another by frequency division. The structure of the sensor and the method to detect the label number and position of the sensor elements that are in contact with obstacles are described, followed by analysis of the circuits and experimental results of the sensor system.**

I. Introduction

Tactile sensors have proven to be effective for collision avoidance control of manipulators especially in the unstructured environment

Manuscript received March 6, 1991; revised March 10, 1992.

Y. Yamada, Nuio Tsuchida, and M. Komai are with the Information and Control Engineering, Toyota Technological Institute, 2-12-1, Hisakata, Tempaku, Nagoya 468, Japan.
K. Shin is with the Production Engineering Department, Daikin Industry Company, 1000-2, Ohtani, Okamoto, Kusatsu, 525 Japan.

IEEE Log Number 9208255.